Time-lapse sonic logs reveal patchy CO_2 saturation in-situ

E. Caspari,[1,2] T. M. Müller,[3] and B. Gurevich[1,2,3]

Received 1 February 2011; revised 17 May 2011; accepted 18 May 2011; published 1 July 2011.

[1] Based on time-lapse sonic and neutron porosity logs from the Nagaoka CO_2 sequestration experiment, a P-wave velocity-saturation relation at reservoir depth is retrieved. It does not coincide with either of the end-member models of uniform and patchy saturation but falls in between even if realistic error estimates for the host rock properties are considered. Assuming a random distribution of CO_2 patches it is shown that the mechanism of wave-induced flow can be evoked to explain this velocity-saturation relation. Characteristic CO_2 patch size estimates range from 1 to 5 mm. Such mesoscopic heterogeneity can be responsible for attenuation and dispersion in the well logging frequency band.
Citation: Caspari, E., T. M. Müller, and B. Gurevich (2011), Time-lapse sonic logs reveal patchy CO_2 saturation in-situ, *Geophys. Res. Lett.*, *38*, L13301, doi:10.1029/2011GL046959.

1. Introduction

[2] Time-lapse seismic monitoring of CO_2 geosequestration requires a sound understanding of phenomena that cause changes in seismic signals. One of these phenomena is the effect of CO_2 saturation on elastic properties of rocks [*Carcione et al.*, 2006; *Vanorio et al.*, 2010]. The seismic P-wave velocity may be strongly dependent on the CO_2 saturation and, therefore, results in a distinct velocity saturation relation (VSR). Two well-known VSRs are the uniform and patchy saturation relationships [*Mavko and Mukerji*, 1998]. These two relationships give the low and high-frequency limits of VSR, respectively, and represent lower and upper bounds such that at a finite frequency the velocity must lie in between these bounds. The variation of velocity with frequency (and corresponding attenuation) are caused by a local fluid flow induced by a passing wave around fluid patches [*Johnson*, 2001; *Tserkovnyak and Johnson*, 2002; *Müller et al.*, 2010]. This wave-induced flow and the resulting dependency of velocity on saturation and frequency are controlled by the geometrical distribution of fluids, and in particular, by the characteristic length scale of the CO_2 patches. Knowledge of this length scale is necessary to predict the time-lapse seismic response. Conversely, knowledge of the acoustic response of a partially saturated medium provides a pathway to estimate the characteristic length scale of CO_2 distribution. CO_2 patch size estimates have been reported on the basis of laboratory ultrasound measurements on partially saturated rock samples [*Lei and Xue*, 2009], however, in-situ estimates remain elusive.

[3] Time-lapse sonic and neutron logs of the Nagaoka CO_2 sequestration experiment [*Konishi et al.*, 2009] provide an opportunity to study the VSR at in-situ conditions in the sonic log frequency band. These logs have been analyzed in previous studies; however, conclusions about the saturation state and corresponding fluid distribution are still a matter of debate [*Xue et al.*, 2006; *Konishi et al.*, 2009]. *Xue et al.* [2006] perform history matching with the sonic logs using the uniform saturation model. On the other hand, *Konishi et al.* [2009] show that the VSR follows a linear trend broadly consistent with the patchy saturation model. However, their VSR trends are rather broad due to strong vertical heterogeneity of the injection interval and random errors in log measurements.

[4] The aim of this paper is to analyze VSRs from the Nagaoka time-lapse logs and to estimate in-situ CO_2 patch sizes from these VSRs. To eliminate the effect of heterogeneity we analyze the time-lapse log data separately for two thin reservoir intervals. We then model the VSR with the 1D and 3D continuous random media (CRM) theories of patchy saturation [*Müller and Gurevich*, 2004; *Toms et al.*, 2007].

2. Time-Lapse Log Data Analysis

[5] In the observation well OB2 at the Nagaoka test site, time-lapse sonic and neutron porosity logs were recorded; 23 logs during a 18 months CO_2 injection period and 14 logs after the injection stopped [*Xue et al.*, 2006]. The averages of the first 13 sonic and neutron porosity logs, recorded before CO_2 breakthrough, are used as baseline data and the logs 17 to 26 as monitoring data (Figure 1). *Sato et al.* [2011] report that the log responses vary with depth in the reservoir zone (1112–1118 m) indicating that this zone is heterogeneous. Therefore, a VSR inferred from log responses of the whole reservoir zone, is probably influenced by variations of rock properties with depth and will mask the true VSR. To eliminate the ambiguity caused by this effect, we analyze only two 0.5 m thick intervals with relatively small depth variations.

[6] The CO_2 saturation is estimated from differences in the time-lapse neutron logs. Given that the neutron log is sensitive to the water content, changes in water saturation caused by CO_2 injection can be used to calculate the CO_2 saturation as follows $S_{CO_2} = (\Phi_b - \Phi_m)/\Phi_b$, where Φ_b and Φ_m denotes the baseline and monitoring neutron porosity, respectively [*Konishi et al.*, 2009].

[7] The baseline logs exhibit strong variations between subsequent runs. Such non-repeatability produces random variations in P-wave velocity and CO_2 saturation with time [*Sato et al.*, 2011]. Since the subsurface has not changed between the runs, these variations are likely to be caused by log measurement errors [*Xue et al.*, 2006]. To minimize the problem of random fluctuations, the data points are

[1]CO2CRC, Bentley, Western Australia, Australia.
[2]Department of Exploration Geophysics, Curtin University, Perth, Western Australia, Australia.
[3]CSIRO Earth Science and Resource Engineering, Bentley, Western Australia, Australia.

0094-8276/11/2011GL046959

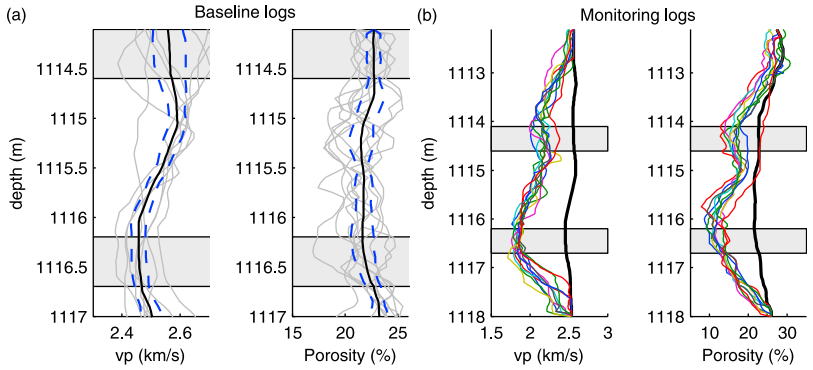

Figure 1. (a) Sonic and neutron porosity baseline logs 1–13 (gray lines), averaged baseline log (black line) and the corresponding standard variation (dashed blue line). (b) Sonic and neutron porosity monitoring logs 17–26 (colored lines) and averaged baseline log (black line). Gray boxes indicate the chosen depth intervals (data from *Konishi et al.* [2009]).

approximated by smooth functions of time for each individual depth. More precisely, we use $S_{CO_2} = S_{\max}(1 - e^{-\alpha t})$, $V_P = V_{P\max} - \Delta V_P(1 - e^{-\beta t})$, where $S_{\max}$ and $V_{P\max}$ are the maximum saturation and P-wave velocity, and ΔV_P denotes the difference between maximum and minimum P-wave velocity. The coefficients α and β are fitting parameters. We note that the use of fitting functions is a simplification as it implies a constant CO_2 supply into the reservoir. This is not necessarily guaranteed as the injection rate was not constant during the injection period [*Xue et al.*, 2006]. However, from *Sato et al.* [2011] we infer that fluctuations in CO_2 saturation and velocity are uncorrelated. This indicates the presence of random fluctuations and justifies our smoothing approach.

3. Velocity-Saturation Relation in Random Media

[8] The behavior between the two limits of uniform and patchy saturation can be explained in terms of the mechanism of wave-induced fluid flow on mesoscopic fluid heterogeneities. Mesoscopic refers to a length scale that is large compared to a typical pore size but small compared to the wavelength. Wave-induced fluid flow causes pressure gradients between patches of different fluids. In the low frequency limit, there is enough time for pressure to equilibrate and the saturation can be considered as uniform. The saturated P-wave modulus H is defined by the Gassmann-Wood (GW) theory

$$H_{\mathrm{GW}} = L + \alpha^2 M\left(K_{f(\mathrm{W})}\right), \quad K_{f(\mathrm{W})}^{-1} = \frac{S_w}{K_w} + \frac{S_{CO_2}}{K_{CO_2}}, \tag{1}$$

where $M = [(\alpha - \Phi)/K_s + \Phi/K_f]^{-1}$ is the fluid storage modulus with $\alpha = 1 - K_d/K_s$, L is the dry P-wave modulus and K_s, K_f, K_w and K_{CO_2} are the grain, fluid, brine and CO_2 bulk moduli, respectively. Specifically, this is true when the characteristic patch size of fluid heterogeneities is much smaller than the fluid diffusion length $\lambda_d = \sqrt{\kappa N/\omega\eta}$, where κ denotes the permeability, η the viscosity, ω the angular frequency and $N = ML/H$. In the high-frequency limit (patchy saturation), there is no pressure communication between the different fluid patches so that fluid communication can be ignored. In this case the saturated P-wave modulus can be obtained from the Gassmann-Hill (GH) theory

$$H_{\mathrm{GH}} = \left[\frac{S_{CO_2}}{H_{sat(CO_2)}} + \frac{S_w}{H_{sat(w)}}\right]^{-1}, \tag{2}$$

where $H_{sat(w)}$ and $H_{sat(CO_2)}$ are the saturated P-wave moduli for each patch. At all intermediate frequencies, wave attenuation and velocity dispersion occur due to wave induced fluid flow and produce a specific VSR. The latter can be modeled by the 1D and 3D continuous random media models of patchy saturation [*Müller and Gurevich*, 2004; *Toms et al.*, 2007].

[9] The 1D model represents a system of alternating CO_2 and brine layers of random thickness while the 3D model represents a system of randomly distributed fluid patches in space. These random variations are described by a normalized autocorrelation function of the fluid bulk moduli. In particular, for an exponential correlation function, the dynamic-equivalent P-wave modulus for the 1D model is

$$\begin{aligned} H_{1D}(\omega) &= H_{\mathrm{GW}}\left[1 + \frac{s}{1 + \frac{2i}{kd}}\right], \\ k &= \sqrt{\frac{i\omega}{\kappa}}\frac{\sqrt{\eta_w N_w}S_w + \sqrt{\eta_{CO_2} N_{CO_2}}S_{CO_2}}{N_w S_w + N_{CO_2} S_{CO_2}} \end{aligned} \tag{3}$$

The degree of inhomogeneity is given by a parameter $s = H_{GH}/H_{GW} - 1$ and the correlation length d describes a characteristic patch size of the medium. The P-wave modulus for the 3D model can be written as

$$\begin{aligned} H_{3D}(\omega) &= H_{\mathrm{GW}}\left[1 + \frac{H_{\mathrm{GH}} - H_{\mathrm{GW}}}{H_h - H_l}\frac{H_{eff} - H_l}{H_{\mathrm{GW}}}\right], \\ H_{eff} &= H_0\left(1 - \Delta_2 - \frac{\Delta_1 k^2 d^2}{(ikd - 1)^2}\right)^2, \\ H_l &= H_0(\Delta_2 - 1)^2, \quad H_h = H_0(1 - \Delta_2 + \Delta_1)^2, \\ k &= \sqrt{\frac{i\omega\eta}{\kappa N}}, \quad \Delta_1 = \frac{L\Delta_2}{H}, \quad \Delta_2 = \frac{\alpha^2 M \sigma_{MM}^2}{2H}, \end{aligned} \tag{4}$$

where H_{eff} is the effective complex P-wave modulus, H_l and H_h the low and high frequency limits derived from H_{eff} and

Table 1. Petrophysical Properties of the Rock and Fluids[a]

Rock	K_g(GPa)	K_d(GPa)	μ(GPa)	ρ_g(g/cm^3)	Φ	κ(mD)	V_p/V_s
Nagaoka (OB2)	27.74	2.5–3.3[b]	2.4–3.3[b]	2.5	0.23	10	1.52[c]
Tako sandstone	38	6	6	2.5	0.25	15	
Fluids		K_f(GPa)		ρ(g/cm^3)		η(Pa * s)	
Brine (Nagaoka)		2.5		1		1e-3	
Brine (Tako)		2.25		0.997		8e-4	
supercritical CO_2 (Nagaoka)		0.0465		0.623		4.4e-5	
supercritical CO_2 (Tako)		0.046		0.62		7e-5	

[a]Rock and fluid properties are taken from *Konishi et al.* [2009], *Xue et al.* [2006] and *Lei and Xue* [2009].
[b]Calculated properties.
[c]*Han et al.* [1986].

σ^2_{MM} the normalized variance of the fluid storage modulus. The average background P-wave modulus H_0 is calculated from Gassmann's equation using an average fluid modulus.

[10] The real part of the P-wave moduli (3) and (4) yield the VSR. It is a function of the wave frequency, the fluid patch size, and the ratio of the permeability and the fluid shear viscosity. The 1D and 3D CRM models constitute two end-member scenarios with respect to patch geometry. Fluid patches are not expected to be perfect layers nor fully isotropic in 3D space but more likely something in between.

4. Velocity-Saturation Relation at Nagaoka

[11] VSR modeling requires the knowledge of the elastic properties of the dry frame. Since the reservoir shows vertical heterogeneity, we calculate the dry bulk modulus K_d from the sonic baseline data (corresponding to 100% water saturated conditions) for each depth rather than using an average value for the whole reservoir. As no S-wave velocity is available, we choose a V_p/V_s ratio from literature data [*Han et al.*, 1986]. This ratio is substituted into Gassmann's equation which is then solved for K_d. The computed dry bulk moduli (2.5–3.3 GPa) are comparable to the values derived by *Xue et al.* [2006] and *Konishi et al.* [2009]. *Xue et al.* [2006] report that the dry properties could not be measured due to the friable nature of the rock. Such a soft rock is favorable for seismic monitoring purposes as then strong time-lapse signals can be expected. The rock and fluid parameters are summarized in Table 1.

[12] The GW and GH bounds for the Nagaoka data are shown in Figure 2. It can be observed that most raw data points (red squares) fall between the uniform and patchy saturation bounds. That is still true if we take into account the standard variation of the baseline logs, indicated by gray lines. Compared to the raw data the smoothed data points (black circles) exhibit less scatter and allow us to define a distinct velocity-saturation trend.

[13] In the next step we model the VSR using the CRM models. Using a typical sonic log frequency and the known permeability and fluid viscosities (Table 1) yields velocity-saturation predictions based on equations (5) and (6) which depend on the correlation length d. For d = 0.1 mm the predictions converge to the GW bound whereas for d = 3 cm the prediction is close to the GH bound. The velocity-saturation trend of the smoothed data follows the predictions of the CRM models for a range of correlation lengths. This in turn allow us to infer characteristic patch sizes of CO_2 by fitting a 1D and 3D CRM model to each point of the smoothed data. The resulting correlation lengths are between 1–5 mm. Figure 2 shows the corresponding VSRs for 1 mm and 5 mm.

[14] Note that the VSR is controlled by the characteristic patch size, which itself can depend on saturation [*Toms-Stewart et al.*, 2009]. However, the VSR trend in Figure 2 appears to be parallel to the CRM lines, indicating no obvious variation of the patch size with saturation. The fluid

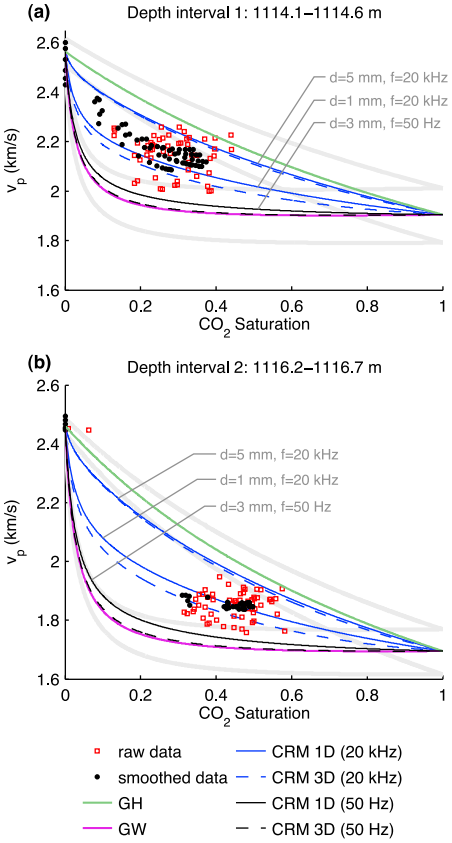

Figure 2. Comparison between theoretical models (GW, GH and CRM) and log data for the (a) first and (b) second depth interval. The gray lines show the deviations of the GW and GH bounds, obtained from the standard variation (non-repeatability) of the repeated baseline logs. The CRM models are displayed for 20 kHz with correlation lengths d of 1 mm and 5 mm (solid and dashed blue curves) and for 50 Hz with d = 3 mm (solid and dashed black curves).

patch sizes inferred from the 3D CRM model are consistently larger compared to those corresponding to the 1D CRM model. This accounts for the fact that wave-induced flow in 1D heterogeneous media occurs in a broader frequency range compared to the 3D situation [*Müller and Gurevich*, 2004]. Furthermore, in the first depth interval, patches are slightly larger than in the second one, which demonstrates that the patch sizes are likely to vary from layer to layer. These layer-dependent patch size variations can originate from variations of other poroelastic parameters (e.g., porosity) across the depth interval. Another possible explanation is that lower CO_2 saturations (first depth interval) are more prone to patchiness than higher CO_2 saturations. This highlights the importance of analyzing the VSR independently for different depth intervals.

5. Discussion and Conclusion

[15] The estimated characteristic size of fluid patches is on the order of a few millimeters. Comparing these estimates with the pore-scale features of a reservoir thin section [*Xue et al.*, 2006] demonstrates that the patch sizes are indeed much larger than a typical pore size. This indicates that wave-induced fluid flow between mesoscopic inhomogeneities may occur at sonic frequencies and therefore strongly controls the velocity-saturation behavior.

[16] Our patch size estimates are consistent with those *Lei and Xue* [2009] inferred from laboratory ultrasound measurements on Tako sandstone using the White-Dutta-Odé model for patchy saturation (1.3–1.5 mm). The petrophysical properties of Tako sandstone and the Nagaoka reservoir are quite comparable (Table 1). The main difference is that the Tako sandstone is well cemented in contrast to the friable reservoir samples from OB2. However, the fluid diffusion lengths $\lambda_d = 0.25$ mm (Tako) and $\lambda_d = 0.65$ mm (Nagaoka) are of the same order of magnitude. This indicates that similar patch sizes can play a role in laboratory ultrasound and sonic log measurements. It shows an intriguing possibility that laboratory fluid injection experiments may be used to simulate in-situ conditions in the sonic frequency band.

[17] In order to understand if heterogeneities of this length scale have any effect in the seismic frequency band, we model the VSR for a frequency of 50 Hz and a correlation length of 3 mm (black lines in Figure 2). The 3D CRM model coincides with the GW limit, whereas the VSR for the 1D CRM model converges slower to this bound as attenuation and dispersion occur in a broader frequency range. Thus, for patch sizes in the millimeter range the GW limit can be used as a first order approximation.

[18] We analyzed two small depth intervals using wireline logging data. Hence, the VSR results are limited by the penetration depth of the log measurements and do not permit any conclusion on fluid distribution on a larger scale. To analyze if attenuation and dispersion play a role at seismic frequencies we estimate a characteristic length scale of the depth variations. First, the depth trend from the sonic monitoring data is removed. Then the autocorrelation of the remaining fluctuations is calculated for each run and a characteristic correlation length of 25 cm is inferred. Heterogeneities of this size could cause dispersion and attenuation at seismic frequencies according to the CRM models. But it has to be further investigated if the magnitudes of the fluctuations reflect random variations of layer properties rather than random noise associated with measurement errors.

[19] **Acknowledgments.** We acknowledge the funding provided by the Australian government through the CRC Program to support CO2CRC research.

[20] The Editor thanks the three anonymous reviewers for their assistance in evaluating this paper.

References

Brie, A., F. Pampuri, A. Marsala, and O. Meazza (1995), Shear sonic interpretation in gas bearing sands, paper 30595-MS presented at Annual Technical Conference and Exhibition, Soc. of Pet. Eng., Dallas, Tex., 22–25 Oct.

Carcione, J., S. Picotti, D. Gei, and G. Rossi (2006), Physics and seismic modeling for monitoring CO_2 storage, *Pure Appl. Geophys.*, *163*(1), 175–207.

Han, D., A. Nur, and D. Morgan (1986), Effects of porosity and clay content on wave velocities in sandstones, *Geophysics*, *51*(11), 2093–2107.

Johnson, D. L. (2001), Theory of frequency dependent acoustics in patchy-saturated porous media, *J. Acoust. Soc. Am.*, *110*(2), 682–694.

Konishi, C., H. Azuma, D. Nobuoka, Z. Xue, and J. Watanabe (2009), CO_2 saturation estimation from P-wave velocity changes by considering patchy saturation, paper presented at Summer Research Workshop, Soc. of Explor. Geophys., Banff, Alberta, Canada, 23–27 Aug.

Lei, X., and Z. Xue (2009), Ultrasonic velocity and attenuation during CO_2 injection into water-saturated porous sandstone: Measurements using difference seismic tomography, *Phys. Earth Planet. Inter.*, *176*(3–4), 224–234.

Mavko, C., and T. Mukerji (1998), Bounds on low frequency seismic velocities in partially saturated rocks, *Geophysics*, *63*(3), 918–924.

Müller, T. M., and B. Gurevich (2004), One-dimensional random patchy saturation model for velocity and attenuation in porous rocks, *Geophysics*, *69*(5), 1166–1172.

Müller, T. M., B. Gurevich, and M. Lebedev (2010), Seismic wave attenuation and dispersion resulting from wave-induced flow in porous rocks—A review, *Geophysics*, *75*, 75A147, doi:10.1190/1.3463417.

Sato, K., S. Mito, T. Horie, H. Ohkuma, H. Saito, J. Watanabe, and T. Yoshimura (2011), Monitoring and simulation studies for assessing macro- and meso-scale migration of CO_2 sequestered in an onshore aquifer: Experiences from the Nagaokapilot site, Japan, *Int. J. Greenhouse Gas Control*, *5*, 125–137.

Toms, J., T. M. Müller, and B. Gurevich (2007), Seismic attenuation in porous rocks with random patchy saturation, *Geophys. Prospect.*, *55*(5), 671–678.

Toms-Stewart, J., T. M. Müller, B. Gurevich, and L. Paterson (2009), Statistical characterization of gas-patch distributions in partially saturated rocks, *Geophysics*, *74*(2), WA51–WA64.

Tserkovnyak, Y., and D. L. Johnson (2002), Can one hear the shape of a saturation patch?, *Geophys. Res. Lett.*, *29*(7), 1108, doi:10.1029/2001GL014709.

Vanorio, T., G. Mavko, S. Vialle, and K. Spratt (2010), The rock physics basis for 4D seismic monitoring of CO_2 fate: Are we there yet?, *Leading Edge*, *29*(2), 156.

Xue, Z., D. Tanase, and J. Watanabe (2006), Estimation of CO_2 saturation from time-lapse CO_2 well logging in an onshore aquifer, Nagaoka, Japan, *Explor. Geophys.*, *37*(1), 19–29.

E. Caspari and B. Gurevich, Department of Exploration Geophysics, Curtin University, GPO Box U 1987, Perth, WA 6845, Australia. (eva.caspari@postgrad.curtin.edu.au; b.gurevich@curtin.edu.au)

T. M. Müller, CSIRO Earth Science and Resource Engineering, GPO Box 1130, Bentley, WA 6102, Australia. (tobias.mueller@csiro.au)